THE ASTRONOMICAL JOURNAL, 121:1522–1532, 2001 March
© 2001. The American Astronomical Society. All rights reserved. Printed in U.S.A.

AN EXTINCTION MAP AND COLOR-MAGNITUDE DIAGRAM FOR THE GLOBULAR CLUSTER NGC 3201

KASPAR VON BRAUN AND MARIO MATEO
Department of Astronomy, University of Michigan, 830 Dennison Building, Ann Arbor, MI 48109-1090; kaspar@astro.lsa.umich.edu, mateo@astro.lsa.umich.edu
Received 2000 October 6; accepted 2000 November 16

ABSTRACT

Differential E_{V-I} variations of up to $\sim$0.2 mag on a scale of arcminutes across NGC 3201 are presented in the form of an extinction map. This map, created by calculating average E_{V-I} values for stars in small subregions of the field with respect to a fiducial region, greatly improves the appearance of the color-magnitude diagram of the cluster. We describe how we implemented this technique in detail with our data for NGC 3201. A comparison between our map and that of the same region extracted from the *COBE* DIRBE reddening maps published by Schlegel, Finkbeiner, & Davis in 1998 (hereafter SFD) displays larger scale similarities between the two maps, as well as smaller scale features that show up in our map but not in the SFD map. Several methods of determining an E_{V-I} zero point to add to our differential extinction map are presented. Isochrone fitting proved to be the most successful one, but it produces an average E_{V-I} for the cluster that is smaller by $\sim$1.5 σ than previously published values. Finally, our results seem to support the statement by Arce & Goodman that the SFD maps overestimate the reddening in regions of high extinction.

Key words: color-magnitude diagrams — dust, extinction — globular clusters: individual (NGC 3201) — methods: data analysis — stars: fundamental parameters

On-line material: color figures

1. INTRODUCTION

We are currently undertaking a survey of approximately 15 Galactic globular clusters (GCs) with the aim of identifying eclipsing binary stars around or below the turnoff point by detecting brightness variations. These systems can provide masses for Population II main-sequence stars. High-quality photometry is essential for obtaining reliable values for surface temperatures, luminosities, ages, etc. Precise extinction determinations are a critical part of obtaining these results from our photometry.

NGC 3201, by chance one of the first GCs we analyzed, is a low-latitude cluster, located at $\alpha_{2000} = 10^{h}36^{m}36\overset{s}{.}8$ and $\delta_{2000} = -46°24'40''$, or $l = 277\overset{\circ}{.}2$ and $b = 8\overset{\circ}{.}6$ (Harris 1996), with a retrograde orbit around the center of the Milky Way. Its nearby location ($d = 5.2$ kpc) and low concentration ($c = 1.31$; Harris 1996) make it an attractive target for photometric studies. Recent studies include those of Da Costa, Frogel, & Cohen (1981), Cacciari (1984), Brewer et al. (1993), Côté et al. (1994), Covino & Ortolani (1997, hereafter CO97), and Gonzalez & Wallerstein (1998, hereafter GW98).

Because of its low-latitude position, the effects of differential reddening across the face of NGC 3201 are quite substantial. The existence of variable extinction was noted in practically all earlier studies of this cluster. Cacciari (1984), for instance, finds an irregular reddening distribution with a variation of $\Delta E_{B-V} = 0.03$ mag in addition to a mean value of $E_{B-V} = 0.21$. GW98 report a range in E_{B-V} of as much as 0.1 mag across NGC 3201. Using spectroscopic data for 18 giants in NGC 3201, GW98 correct for the color spread by modeling the reddening in E_{B-V} as a plane in α and δ.

Recently published dust infrared emission maps by Schlegel, Finkbeiner, & Davis (1998, hereafter SFD) seem to indicate, however, that the dust distribution in the region of NGC 3201 is too clumpy to be fitted by a linear function in position, even on a scale of arcminutes (see below, Fig. 6).

In this work, we attempt to remove the differential reddening across the cluster by using our high-quality VI photometry. Our procedure is, in principle, similar to the one used by Kaluzny & Krzeminski (1993) and Piotto et al. (1999). It aims to find the average ΔE_{V-I} for subregions of the cluster field of approximately 1 arcmin^2 in size, with respect to a fiducial region in the cluster, where little or no differential reddening is apparent and the overall E_{V-I} is small compared to the rest of the cluster. The pixel size (resolution) of this extinction map is approximately one-fourth of the size (in area) of the SFD maps. Since the SFD maps are based on infrared emission from dust, our map will provide an independent check of whether, if at all, they tend to overestimate reddening, as was suggested by, e.g., Arce & Goodman (1999) for regions with $A_V > 0.5$ mag.

Our results indicate variations in E_{V-I} of up to $\sim$0.2 mag. Differential reddening this strong can wreak havoc with photometric and spectroscopic studies of cluster stars. The inherent uncertainties in the various parameters of the color-magnitude diagram (CMD; e.g., magnitude and color of the main-sequence turnoff [MSTO], horizontal branch features, etc.) are greatly amplified. Moreover, one can "detect" age or surface temperature gradients where in reality there are none. To give an example of the magnitude of the effect, we use the recently published color-temperature relations by Houdashelt, Bell, & Sweigart (2000). The effective temperature of a solar-metallicity, main-sequence star with $V-I \sim 0.8$ would vary by approximately 600 K for a differential reddening effect of $E_{V-I} \sim 0.2$ mag, which in turn could lead to errors in the metallicity determination.

Using our internal dereddening technique, we obtain a high-quality, deep-photometry CMD of NGC 3201 comprising approximately 90 600 s exposures, as well as some shorter ones, all using the V and I bands.

Our observations and data reductions, as well as the

details of our internal dereddening method, are documented in § 2. Section 3 contains our results concerning the reddening map and the CMD of NGC 3201. Finally, we discuss the determination of the reddening zero point of our extinction map in § 4 and give a brief summary of our work in § 5.

2. OBSERVATIONS, DATA REDUCTION, AND INTERNAL DEREDDENING

2.1. *Observations and Basic Data Reductions*

The NGC 3201 observations were obtained during the nights of 1998 April 26 through 1998 May 6 at the Las Campanas Observatory's 1 m Swope Telescope, using Johnson-Cousins *VI* filters and a SITe 1 2048^2 CCD with a field of view of 23.'5 on a side. Table 1 gives the number of epochs we observed for different exposure times, which were chosen to cover a larger magnitude range in the CMD.

The initial processing of the raw CCD images was done with the routines in the IRAF[1] CCDPROC package. For each night, 10 bias frames were combined for the bias subtraction. The *V*-band flats were produced by combining between four and six twilight flat images per night. All *I*-band data were first flattened, using an image composed of 15 individual *I*-band dome flats, and then divided by a normalized, dome-flattened, dark-sky flat, which itself was created by median-averaging approximately 40 individual blank-sky fields. Finally, the *I*-band images were corrected for fringing by subtracting a fringe image, which was created by subtracting the mean pixel value of the dark-sky flat from the dark-sky flat image itself.

The processed data were reduced using DoPHOT (Schechter, Mateo, & Saha 1993) in "fixed-position mode," in which the positions of stars are fixed (after correcting for global frame-to-frame shifts, as well as small distortions) to the positions measured on a deep-photometry template image, obtained by coadding the ~ 15 best seeing frames.

The photometric results for every star were averaged over all frames with the same exposure time to obtain the final magnitude for the star under investigation. For the 600 s exposures, our only requirement was that a star appear in more than 75% of the epochs. The 60 s images were taken to complete the CMD in the brighter regions; we only took magnitudes from these exposures of stars that were saturated in the 600 s exposures. The same procedure was followed for the 10 s frames. Aperture corrections were applied by calculating one constant value for the whole chip after we found little dependence upon position on the CCD. The data from the shorter exposures were shifted to the photometric system of the 600 s exposures using nonsaturated stars in common.

During our two consecutive photometric nights (1998 May 2 and 3), we obtained a total of more than 140 observations of various Landolt (1992) standard stars, which covered a range of $-0.2 < V-I < 2.2$ in color, as well as $1.15 < X < 1.55$ in air mass. Using the IRAF PHOTCAL package, we applied a single standard star solution for data from both nights of the form

$$V = v + a_0 + b_0 X_v + c_0(v - i) \quad (1)$$

$$V - I = a_1 + b_1 X_i + c_1(v - i)\,, \quad (2)$$

where a_j, b_j, and c_j are the fitted constants, $X_{\rm filter}$ is the air mass of the exposure taken with the respective filter, the lowercase magnitudes are instrumental, and the uppercase ones are the known magnitudes of the standard stars. The rms error was 0.007 and 0.016 mag for V and $V-I$, respectively.

Astrometry was performed by identifying 59 US Naval Observatory (USNO) reference stars (Monet et al. 1998) in NGC 3201 and using the IRAF IMAGES package for the coordinate transformation. A linear fit in x and y produced errors around 0.''2, consistent with the USNO precision. The tangent point of the transformation was $(x, y) = (962.7, 934.2)$ and corresponds to $\alpha_{2000} = 10^{\rm h}17^{\rm m}31^{\rm s}.2$ and $\delta_{2000} = -46°24'11''$. The rotation of x and y with respect to α and δ was 91.°23, and the pixel scale came out to be 0.695 pixel arcsec^{-1}. These results enabled us to create the reference grid in Figure 3 (see below).

2.2. *Mapping the Differential Reddening*

At this point in the data reduction we were in the possession of a fully calibrated CMD whose main sequence appeared exceptionally broad (see below, Fig. 8). After ruling out a number of possible instrumental causes for this effect and noting a clear dependence of the appearance of the main sequence on the positions of stars on the CCD (illustrated in Fig. 1), we concluded that the underlying cause for the broadness of our main sequence was differential extinction across the field of view. This seemed especially sensible given the low-latitude location of NGC 3201 and motivated us to create a reddening map, since our binary star data were not useful without this correction. To create such a map for NGC 3201, we developed the steps described below (see also Fig. 2):

1. A fiducial region was chosen in which (*a*) very little or no differential reddening occurred, i.e., where the main sequence appeared narrow; (*b*) the overall E_{V-I} was very small with respect to the rest of the field of view; and (*c*) there were enough stars in the field to obtain a statistically reliable fit to their positions on the CMD. The coordinates of this fiducial region are approximately $10^{\rm h}16^{\rm m}26^{\rm s} < \alpha_{2000} < 10^{\rm h}16^{\rm m}53^{\rm s}$ and $-46°31'21'' < \delta_{2000} < -46°26'44''$ (see Figs. 3–7).

2. A high-order polynomial was fit to the main-sequence stars with $18 < V < 21$ and $0.7 < V-\mathrm{I} < 1.4$ in the fiducial region using algorithms supplied by R. Dohm-Palmer (2000, private communication), which enabled us to separate the main-sequence stars from background stars in the CMD, and by Press et al. (1992), which provided the least-squares fit to the data (see Fig. 2).

3. We divided the field of view into subregions of different sizes in order to have a sufficient number of stars in each

[1] IRAF is distributed by the National Optical Astronomy Observatories, which are operated by the Association of Universities for Research in Astronomy, Inc., under cooperative agreement with the NSF.

TABLE 1

NUMBER OF EPOCHS VERSUS EXPOSURE TIMES

Filter	10 (s)	60 (s)	600 (s)
V.....	10	12	46
I	10	12	43

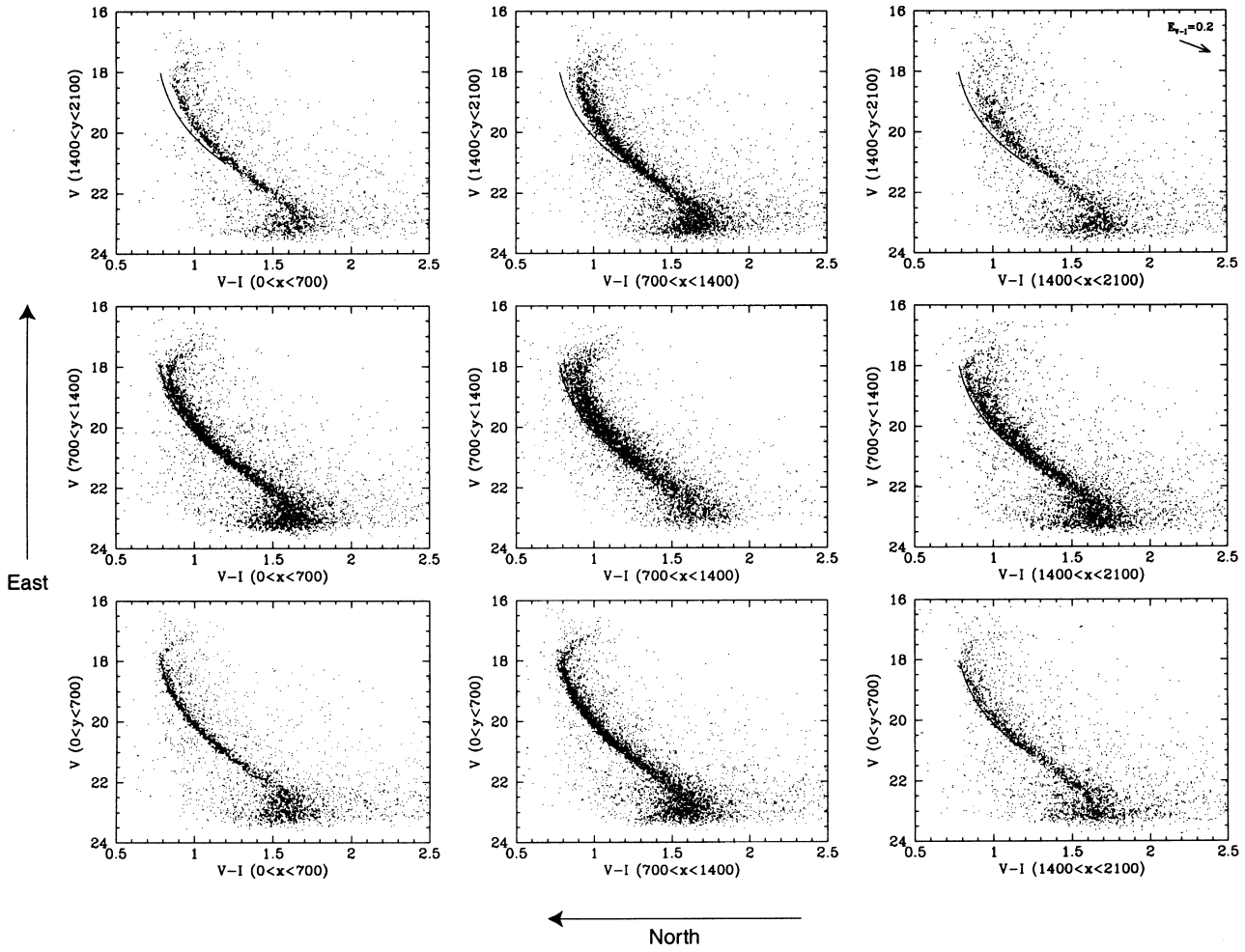

FIG. 1.—"Raw" (calibrated but before dereddening) CMDs of nine subregions of the field of view of NGC 3201. The x and y ranges of the respective subregion are given on the axes of each individual CMD. Here $x = 0$, 700, 1400, and 2100 approximately correspond to $\delta_{2000} = -46°13'03''$, $-46°21'09''$, $-46°29'16''$, and $-46°37'22''$, respectively; $y = 0$, 700, 1400, and 2100 approximately correspond to $\alpha_{2000} = 10^h16^m27^s$, $10^h17^m14^s$, $10^h18^m01^s$, and $10^h18^m48^s$, respectively. The directional arrows on the bottom and the left of the image show the approximate orientation of the CCD. The varying appearance and broadness of the main sequence as a function of position clearly indicates the differential reddening across the field of view. The line through the CMDs represents the best fit through the data points in the fiducial region $1200 < x < 1600$ and $0 < y < 400$ (described in § 2.2, item 1). It is apparent that not only is there less differential reddening in that region (tight main sequence), but also the overall E_{V-I} is low. The reddening vector for $E_{V-I} = 0.2$ is shown in the top right panel.

region. Toward the outer parts of the field, the stellar density decreases. As a result, the sizes of the subregions increase. The inner subregions are all the same size (100 × 100 pixels; see Fig. 3).

4. For each of these regions, every star falling between $17.9 < V < 21.1$ and $0.65 < V-I < 1.45$ was incrementally moved along the reddening vector defined by the relations in Cardelli, Clayton, & Mathis (1989) until it intersected the fit (see Fig. 2).

5. The statistical biweight (see Beers, Flynn, & Gebhardt 1990) of all these incremental shifts of the stars in a given subregion was then calculated, outliers (0.9 σ) were removed, and it was recalculated. This provided the value of the total shift along the reddening vector for each star. Since the slope of the reddening vector for a standard extinction law is known (1.919; see Cardelli et al. 1989), the differential E_{V-I} for each star corresponds to the $V-I$ component of the vector described above (Fig. 2).

6. For six of the 100 × 100 pixel subregions, as well as one 200 × 300 pixel subregion on the extinction map shown in Figure 3, too few stars were present to calculate the average reddening. For these cases, we calculated E_{V-I} by simply averaging the reddening values of all the neighboring subregions.[2]

7. Our error analysis for the shifts described above involved the following:

a) We created an error ellipse for every star defined by the values of the associated errors (as returned by DoPHOT) in color and magnitude.

b) Since the color and magnitude errors are correlated, the error ellipse is tilted, with the tilt angle and the lengths of the semimajor and semiminor axes functions of σ_V and σ_{V-I}.

[2] In this process, every 100 × 100 subregion was treated individually, even if it was a part of a larger one. That is, for the 200 × 300 region just south of the northeast corner of the field of view in which the number of stars was too low to obtain a reddening value, the above procedure was applied six times.

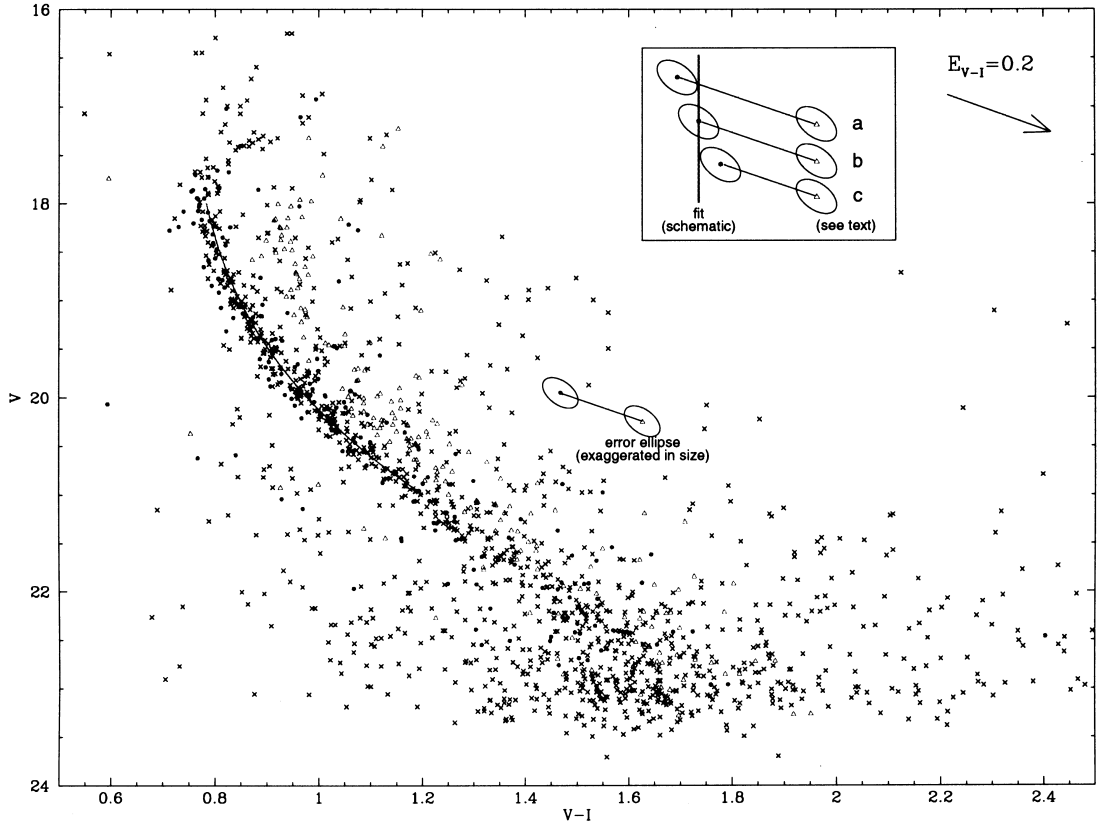

FIG. 2.—Dereddening procedure used in this paper. The triangles represent stars in the subregion $700 < x < 800$ and $800 < y < 900$ (approximately $10^h17^m21^s < \alpha_{2000} < 10^h17^m28^s$ and $-46°21'07'' < \delta_{2000} < -46°22'16''$) before being dereddened; the filled circles represent the same stars after the dereddening along the reddening vector shown in the top right corner of the figure. The crosses are the stars in the fiducial region (mentioned above) in which none or very little differential reddening is taking place. The fitted polynomial with range 18 < mag < 21 is visible as the curve through the fiducial region data points. The reddening for this region is close to $E_{V-I} = 0.2$, with respect to the average of the fiducial region. The tilted error ellipses, described in § 2.2, item 7 and greatly exaggerated in size, are shown to illustrate our dereddening method, which is schematically outlined in the box to the upper right. The straight line represents the fit through the data points in the fiducial region. Examples represent (*a*) the "point of last contact" of the error ellipse with the fit, (*b*) the shift from the original data point until it intersects the fit, and (*c*) the "point of first contact" between the error ellipse and the fit. [*See the electronic edition of the Journal for a color version of this figure.*]

c) One average tilt angle was obtained for every subregion under investigation by averaging the results for the individual stars. For every subregion, this angle was approximately $35° \pm 4°$. The semimajor and semiminor axes for every subregion were obtained in the same way, so that every star in a given subregion has the same error ellipse associated with it in the center.

d) This error ellipse was shifted, along with its respective star, during the dereddening process described above in items 4 and 5. The "point of first contact" (pfc), i.e., the point at which the error ellipse first touches the fit through the data in the fiducial region, as well as the "point of last contact" (plc), represent the respective 1 σ deviation points (see Fig. 2).

e) These two contact points are not necessarily symmetric about the reddening value of the star (center of error ellipse), but to increase the readability of this publication, we calculated the mean pfc and plc for a given subregion, and then their average distance from the center of the ellipse, so that $\sigma_{\rm ellipse} = 0.5(\rm pfc - plc)$.

f) The final error estimate for each subregion ($\sigma_{E_{V-I}}$), given as the lower number in each of the pixels in Figure 4, is then obtained by adding in quadrature $\sigma_{\rm ellipse}$ and the error in the mean of the shifts of all the stars in the subregion under investigation.

3. RESULTS

3.1. *Extinction Map and Comparison with SFD Map*

Figure 3 summarizes the results of our internal dereddening procedure. Darker regions correspond to higher reddening, with respect to the average reddening taking place in the fiducial region described in § 2.2, item 1. For reference purposes, we included the approximate locations of this fiducial region and the core radius of NGC 3201, as well as a coordinate grid. The average E_{V-I} relative to the fiducial region is 86 mmag, with a standard deviation of 61 mmag. The individual subregions' E_{V-I} values in millimagnitudes (relative to the average reddening in the fiducial region) are shown as the top number in each of the pixels in the grid of Figure 4. The bottom number in each pixel corresponds to the error in the mean for the corresponding E_{V-I} value. In addition, we included an image of NGC 3201 (Fig. 5) to indicate the locations of the fiducial region and the core radius of the globular cluster.

At this point, these reddening values are all relative to our fiducial region, which itself is suffering some mean interstellar extinction. The procedure described cannot determine the absolute reddening zero point. Thus, we had to introduce additional information, derived from previous studies, to calculate this zero point. The discussion of this process is given in § 4.1.

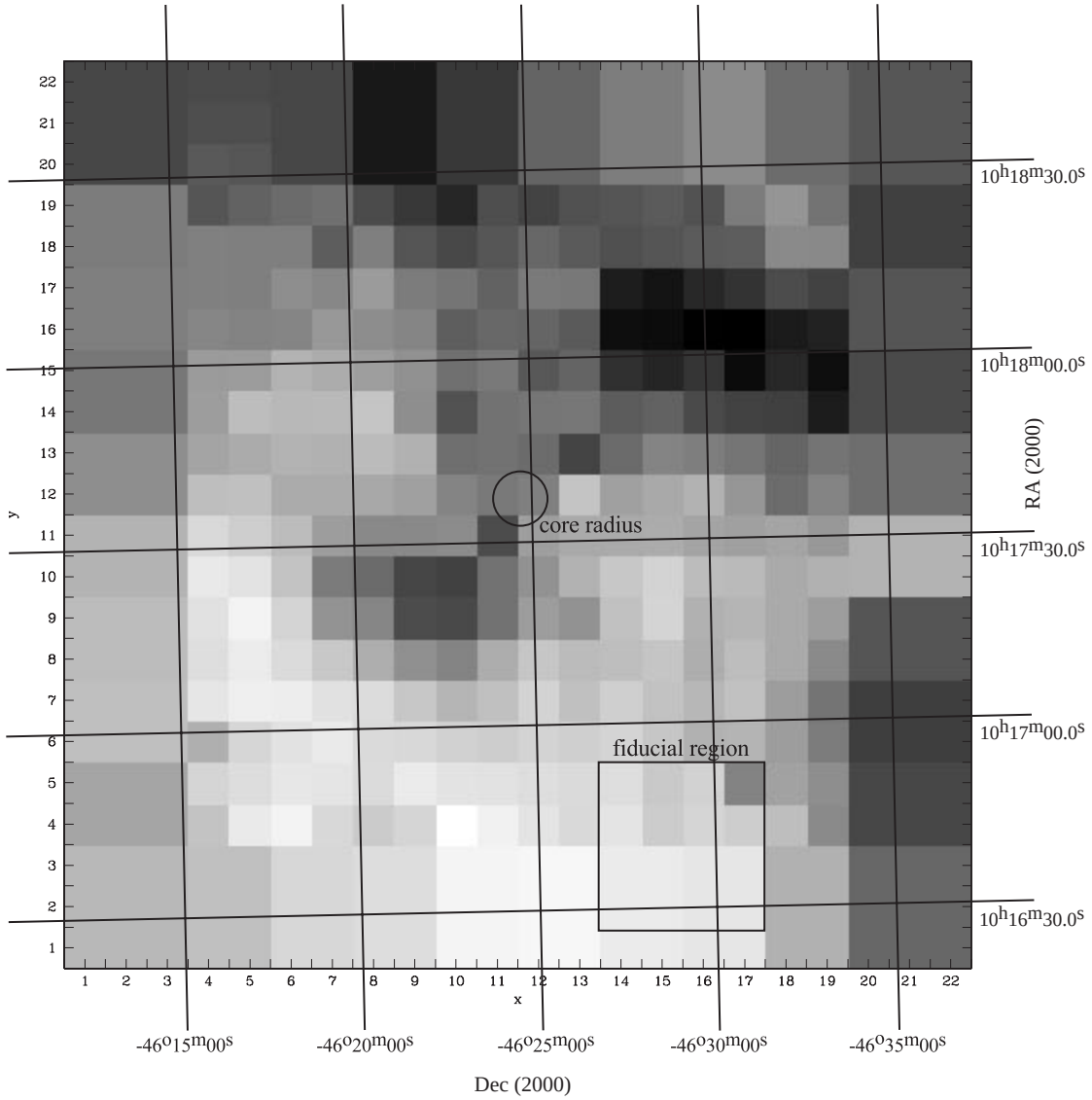

FIG. 3.—Extinction map. East is up, north is to the left. The darker the color of a subregion, the more extinction is occurring in it (see Fig. 4). Note the "ring" of larger subregions (with lower density of stars) around the center of the field of view. The size of every small subregion is approximately 70″ on a side. For reference, we included an illustration of the core radius of NGC 3201 (from Harris 1996) around the location of the cluster center on the extinction map, as well as the location of the fiducial region described in § 2.2. Furthermore, we overlaid a grid for coordinate reference. The coordinate axes x and y correspond to those used in Fig. 4. The average reddening, with respect to the extinction occurring in the fiducial region, is $E_{V-I} = 86 \pm 61$ mmag.

As a first step, we subtracted our extinction map from the SFD map of the region of NGC 3201. The SFD map of the cluster region is shown in Figure 6 with the same orientation and size as Figure 3. Once again, darker regions correspond to higher extinctions. We added the location of the fiducial region for reference. The average E_{V-I} of the SFD map is 487 mmag, with a standard deviation of 59 mmag.

A first comparison indicates that, while the larger scale structure is the same for both extinction maps (in particular, the obscuration ridge extending from the top left part of the image to the right center part of it), our map shows smaller scale features that are not present in the SFD maps. These features are visible in the difference image in Figure 7, whose orientation and size is once again identical to the other figures. Darker regions correspond to places where our data indicate the presence of dust that does not show up in the SFD map; lighter regions show good agreement between the two maps. The average E_{V-I} of this difference map is 401 mmag, with a standard deviation of 46 mmag (significantly smaller than the standard deviation of both our extinction map and the SFD map). This lower standard deviation is an indication that both our map and the SFD map of the region of NGC 3201 are tracing many of the same features in the foreground extinction along the line of sight to the globular cluster.

The smaller scale features present in our map but absent in the SFD map are certainly worth further attention. At this point, we are not entirely confident that we can give a definite reason for the discrepancies, but some potential reasons could be the following:

1. The smaller scale features that are not in the SFD maps might have been smoothed out by the lower resolution of the IR observations used to create the maps.
2. The temperature of the dust producing the smaller scale features was outside the detection range of the instru-

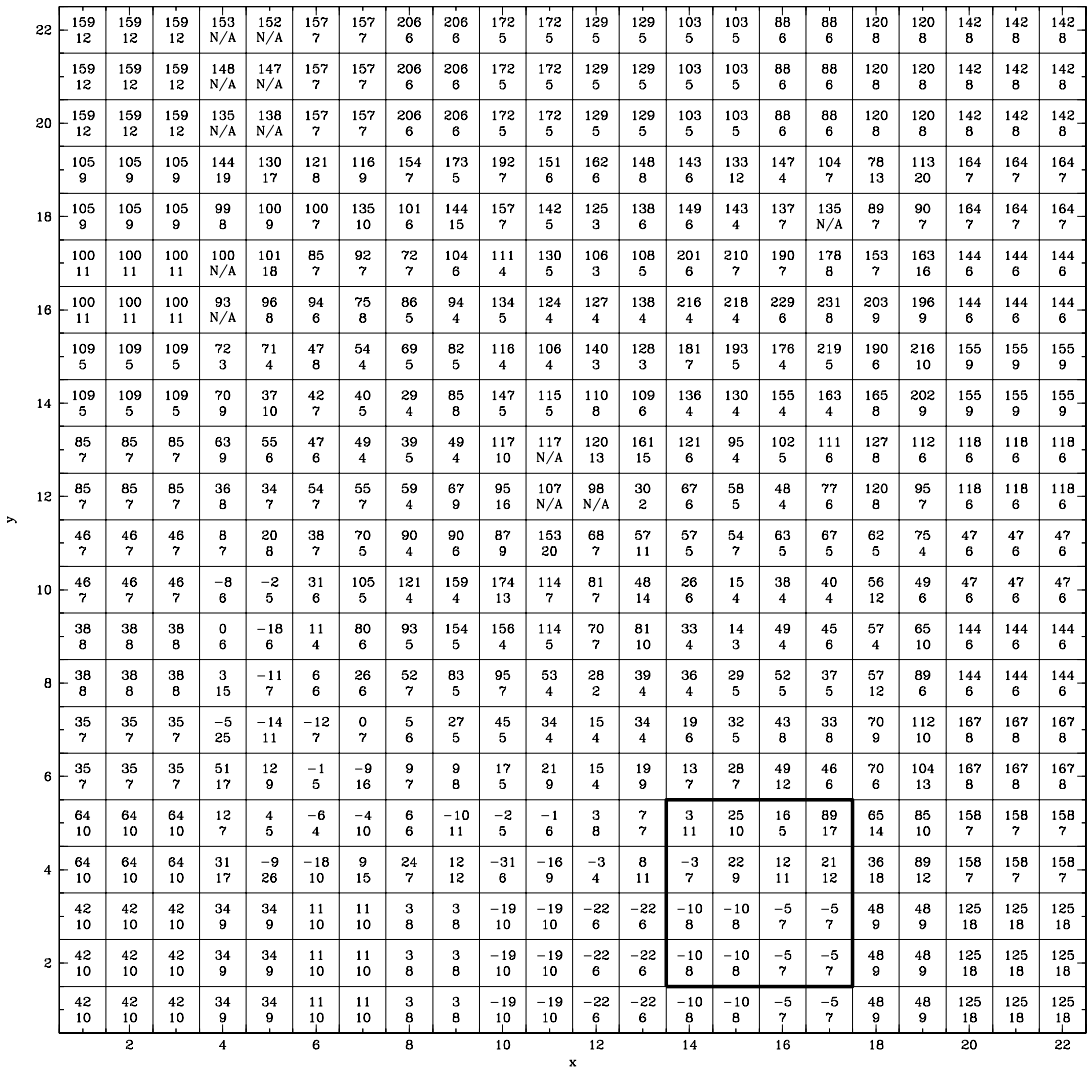

FIG. 4.—E_{V-I} values, with respect to the fiducial region, for the individual pixels of our reddening map in millimagnitudes. The pixels correspond to the subregions in Fig. 3, with the respective values for x and y coordinates. The top number in every pixel is the value for E_{V-I} obtained with the method outlined in § 2.2. The bottom number is the associated error, as described in § 2.2, item 7. The pixels in which the error value is listed as N/A are the ones with an insufficient number of stars, so the reddening results were obtained by interpolation from neighboring values (see § 2.2, item 6). For reference to Figs. 3, 5, 6, and 7 (same orientation), the location of the fiducial region is indicated in the bottom right part of the figure. The average reddening with respect to the mean reddening occurring in the fiducial region is $E_{V-I} = 86 \pm 61$ mmag. To obtain a map of absolute reddening values, an E_{V-I} zero point has to be added to the data. We discuss the various zero points we examined in § 4.1. Finally, to obtain an absolute value for E_{B-V}, one needs to multiply the absolute (i.e., including the zero point) E_{V-I} value by 0.6468 (Cardelli et al. 1989).

ment used to collect the data for the SFD maps. This way, they would still show up in our analysis.

3. The dust we are seeing is actually part of the globular cluster itself[3] and was therefore not picked up in the SFD maps.

3.2. *Photometry and CMD*

Figure 8 contains the raw CMD (no dereddening applied) for NGC 3201. To illustrate the effects of our dereddening method, we show, in Figure 9, the CMD after applying the extinction map (differential reddening correction) to the data. The data points are now all shifted to the CMD location of the stars in the fiducial region; that is, no absolute reddening zero point has been applied. The improvement is quite stunning. The width of the main sequence of Figure 9 has, by applying the differential reddening map, decreased to a fraction of its former value in Figure 8. The subgiant branch, which was hardly visible at all in the raw CMD, is now well traced out by the data points. Even the horizontal branch, although sparsely populated in both CMDs as a consequence of the saturation effects of the bright stars in the field, is narrower in the differentially dereddened CMD.

4. THE REDDENING ZERO POINT OF OUR EXTINCTION MAP FOR NGC 3201

4.1. *Comparing the MSTO Color with Previous Studies*

To make our reddening map (Fig. 4) a useful tool, we need to determine the reddening zero point to add to the E_{V-I} values in the grid. As mentioned above, this could not

[3] The phenomenon of dust inside globular clusters was discussed by, e.g., Forte et al. (1992).

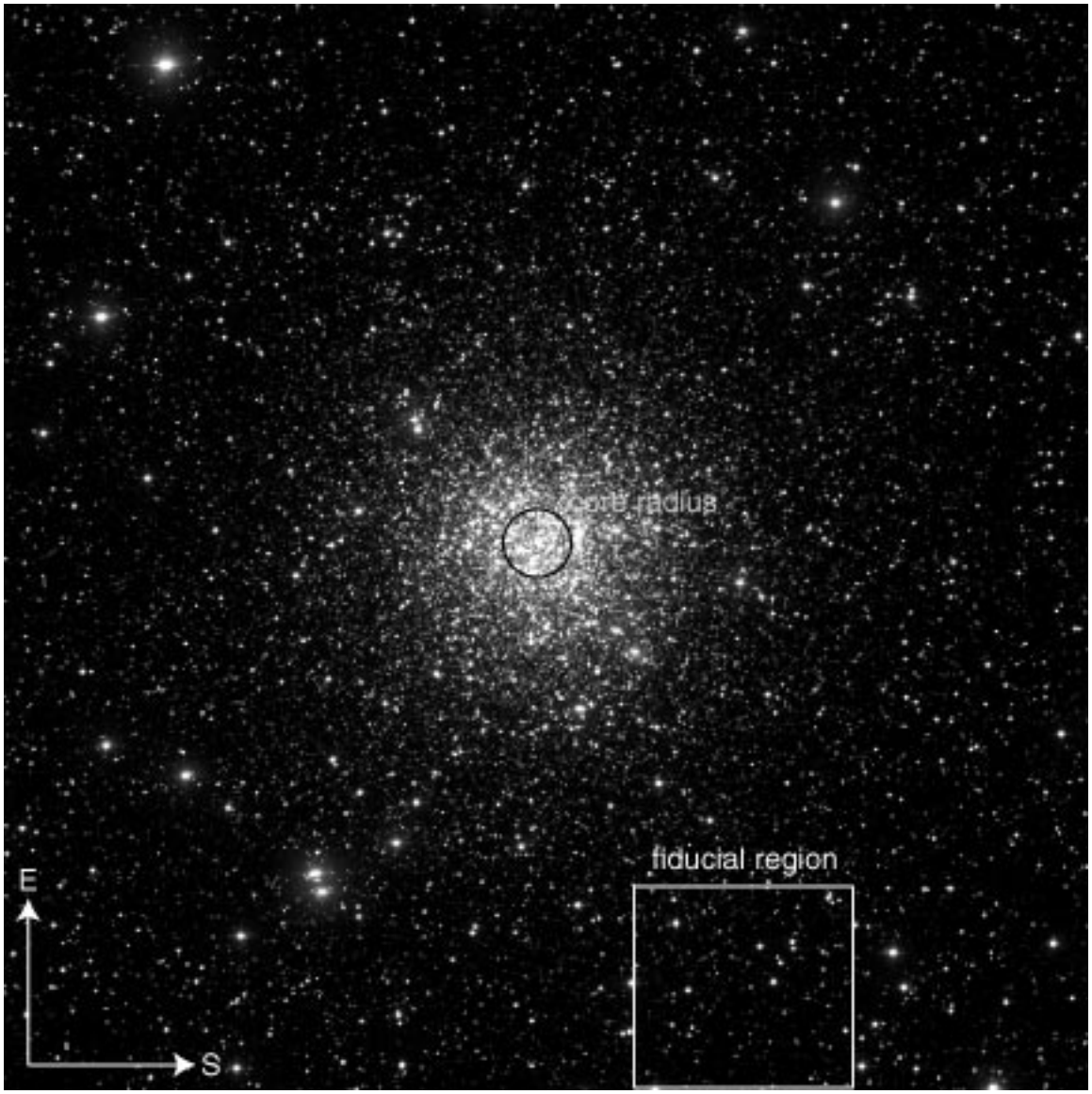

FIG. 5.—Image of NGC 3201 with illustration of core radius and location of fiducial region for purposes of comparison with Figs. 3, 4, 6, and 7. The size of the field of view shown in this figure is about 81% (area) of the field of view of the figures mentioned above. [*See the electronic edition of the Journal for a color version of this figure.*]

be done using our data alone. To be able to use results from previous studies for the calculation of this zero point, an agreement between our photometry results and the corresponding literature values is necessary. When comparing MSTO color, however, one needs to consider that different parts of the field of view are reddened by different amounts, as we showed in our extinction map (Fig. 3).

We estimated our MSTO magnitude, $V_{\rm TO}$, to be 18.2 and the MSTO color, $(V-I)_{\rm TO}$, to be around 0.88 mag; both were determined by eye from the raw photometry CMD (Fig. 8).

These values were compared with the results of Rosenberg et al. (2000, hereafter RB00) and CO97. RB00 find $V_{\rm TO} \sim 18.2$ and $(V-I)_{\rm TO} \sim 0.92$; both values are again determined by eye. CO97 report $V_{\rm TO} \sim 18.15$ and $(B-V)_{\rm TO} \sim 0.65$ (tabulated). Using their reddening estimate of $E_{B-V} \sim 0.22$, the relations in Cardelli et al. (1989), and a set of isochrones provided by Don VandenBerg for [Fe/H] $= -1.41$ (D. VandenBerg 2000, private communication; based on evolutionary models by VandenBerg et al. 2000; hereafter VDB), the CO97 value for $(V-I)_{\rm TO}$ can be calculated to be approximately 0.93.

One discrepancy between our results and these literature values is, therefore, that our value for $(V-I)_{\rm TO}$ is approximately 0.05 mag bluer than what is quoted by the authors mentioned above. The existence of variable reddening may be a likely explanation for this discrepancy, especially when one considers which part of the cluster was observed.

RB00 concentrate on the southern and eastern parts of the cluster for their longer exposures and the center of NGC 3201 for their shorter exposures. These three regions are, according to our reddening map (Fig. 3), regions of higher extinction with respect to our fiducial region.

CO97 observe regions just to the north and west of the cluster center and the cluster center itself. While the north and west regions suffer only low reddening (Fig. 3), the area within $\sim 7'$ to the north and west of the cluster center is obscured by a smaller feature not visible in the SFD map

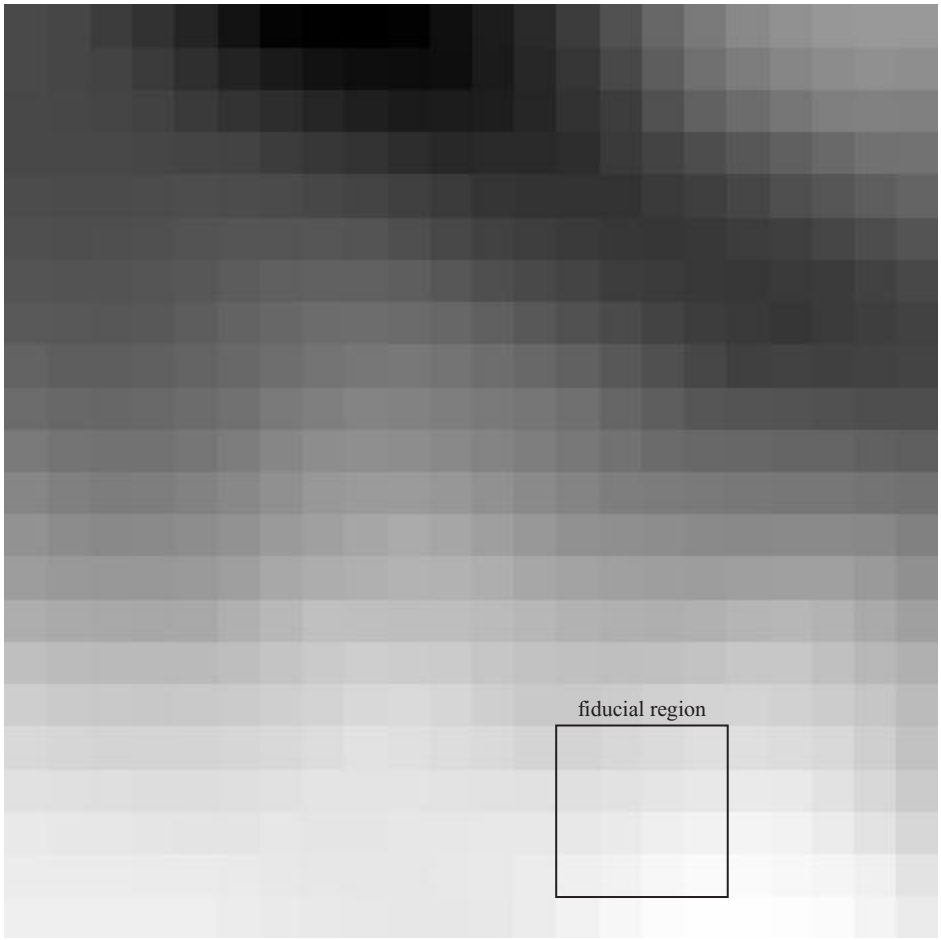

FIG. 6.—Graphical representation of the SFD data in the region of NGC 3201. The location of our fiducial region is given for reference; the orientation of the map is the same as in Figs. 3, 4, 5, and 7. Common features are easily recognizable, such as the ridge of obscuring material extending from the top left part of the map to the right center. A number of smaller scale features, however, do not show up on the SFD map (see Fig. 7). The average reddening is $E_{V-I} = 487 \pm 59$ mmag.

(see Fig. 6). At least five of seven CO97 fields are very likely affected by this dense obscuration feature.

While a quantitative (star by star) magnitude comparison between our data and the data obtained by RB00 and CO97 is not possible, we conclude that their estimates for the MSTO color could very well be influenced by the fact that the regions they observed were subject to an extinction somewhat higher than the average value over our field of view.

We note that these comparisons focus on the MSTO colors; the vertical nature of the MSTO makes it difficult to compare the V magnitude of the MSTO at sufficiently high precision.

4.2. *Basic Isochrone Fitting and Determination of Reddening Zero Point*

We examined three different possibilities for finding the E_{V-I} zero point to add to our extinction map. All three methods are outlined below. For each case, it is worth pointing out that a direct comparison with literature values should be taken with caution, since usually only a single numerical value for the reddening is given, whereas our result is a reddening matrix in which every single element needs to be added to a zero-point offset.

4.2.1. *Using Isochrone Fits*

Simultaneously fitting age, distance, and reddening to the aforementioned set of VDB isochrones produced the fit shown in Figure 10. It should be noted that since the point of this publication is outlining our dereddening method, as well as creating an extinction map for NGC 3201, we only performed some basic isochrone fitting here. For an estimate of [Fe/H], we adopted the isochrone with metallicity closest to the GW98 value of -1.42.

For the fit of Figure 10, [Fe/H] $= -1.41$, $d \sim 4.5$ kpc, the age is 18 Gyr, and the E_{V-I} zero point to be added to the values in Figure 4 is 0.15 mag. The age is clearly on the high end of things, but the 18 Gyr isochrones produced by far the best fits, even when [Fe/H] and the distance were slightly modified. The value for the distance is slightly below the one quoted by Harris (1996) but fairly close to the two values derived by CO97 using slightly different methods.

When adding the mean E_{V-I} of our reddening map (86 mmag) to the zero point, the average E_{V-I} for the cluster is approximately 0.24, which is slightly below the estimates of, e.g., Cacciari (1984), whose E_{V-I} is 0.32, and Harris (1996) and RB00, who quote the same value.

To justify our choice of isochrone parameters and eliminate the possibility of multiple factors conspiring against us

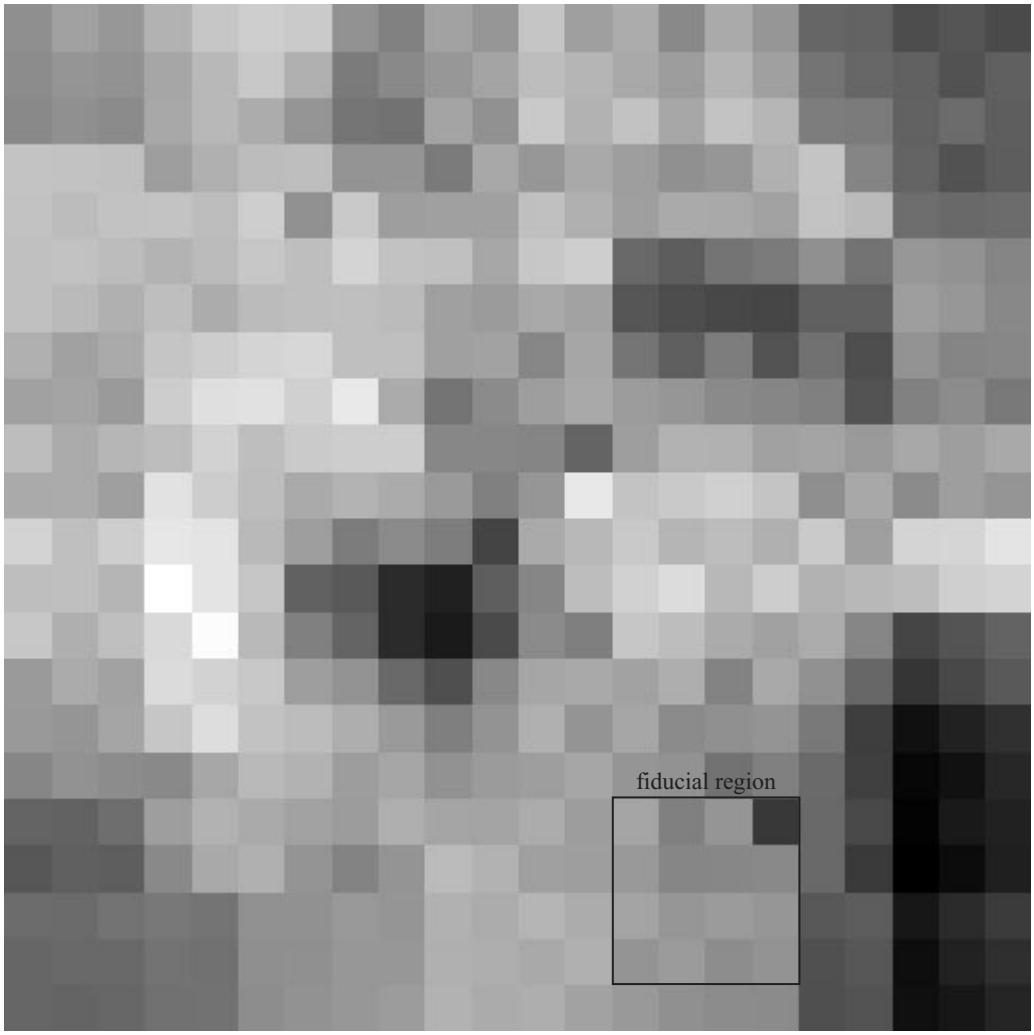

FIG. 7.—Difference plot between our extinction map (Fig. 3) and the SFD map (Fig. 6), with the same orientation. Darker regions correspond to areas where our map indicates more obscuration relative to the average value than the SFD data; lighter regions are places where the two maps agree very well. The average reddening is $E_{V-I} = 401 \pm 46$ mmag, which corresponds to the SFD map zero point (see § 4.2.2). Note that the standard deviation is lower than that of the SFD map and our extinction map.

in the attempt to find a good isochrone fit to the data, we illustrate, in Figure 11, what the CMD would look like if we were to strictly adopt literature values from Harris (1996) ([Fe/H] = −1.58, $E_{V-I} = 0.325$, and $d = 5.2$ kpc). Plotted on top of the data are a pair of isochrones, with respective ages 12 and 14 Gyr.[4] The agreement between data and fit is not as good as in Figure 10.

4.2.2. *Using SFD Maps*

As stated in § 3.1, the mean E_{V-I} of the difference map between the SFD and our data is 401 ± 46 mmag. The average E_{V-I} value for this difference map corresponds to the E_{V-I} zero point to be added to our data to obtain absolute reddening values.

Calculating the total reddening in this fashion gives $E_{V-I} \sim 0.49$, which is significantly higher than the literature values. Furthermore, using the isochrones mentioned in the previous subsection, we were not able to produce a fit to the data due to the fact that E_{V-I} was too high.

4.2.3. *Using RR Lyrae Stars*

Another method of attempting to find a reddening zero point is to simply adopt one from the literature and model the thus dereddened data with a set of isochrones. Here, we took Cacciari's (1984) value of $E_{V-I} \sim 0.32$, which she calculated using RR Lyrae stars. Since this corresponds to the average reddening for the whole cluster, we had to subtract the mean E_{V-I} of her RR Lyrae stars (in our field of view) with respect to our fiducial region. This value turned out to be 79 mmag.

We failed, however, to find a good isochrone fit to the dereddened data, as is shown in Figure 12. To get the MSTO points of the data and the isochrone to agree, we had to lower [Fe/H] to −2.01, a value quite a bit below literature values, such as −1.41 (GW98) or −1.58 (Harris 1996). The distance modulus here is 13.4, and the age is 14 Gyr. As one can easily see, the fit fails to hit the subgiant branch because of the "young" isochrone age of 14 Gyr. Older age isochrones could not be shifted far enough

[4] To have a valid basis for comparison, we needed to apply an E_{V-I} zero point of 0.325 − 0.086 = 0.239 to the differentially dereddened data, in which 0.325 is the Harris (1996) E_{V-I} value and 0.086 is the mean E_{V-I} value of our extinction map.

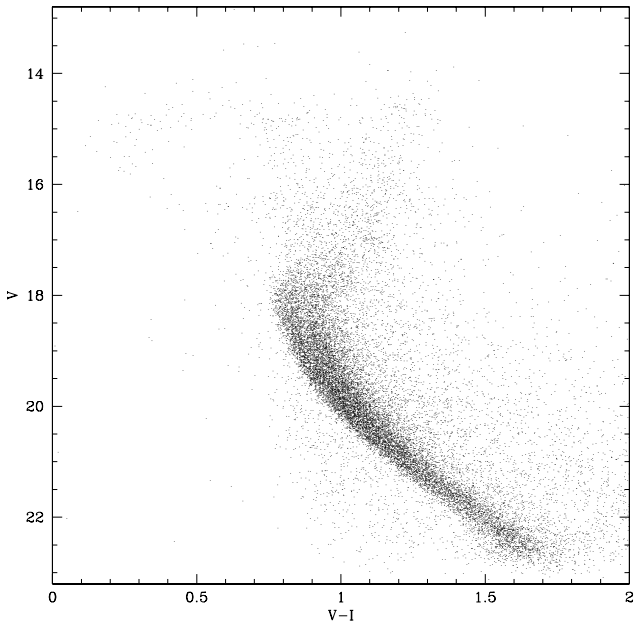

FIG. 8.—Raw CMD of NGC 3201 before applying any dereddening

toward the dereddened MSTO location to produce a fit, even when the metallicity was lowered to the lowest available value of −2.31.

4.2.4. *Comments on the Adopted Reddening Zero Point*

Given that we were not able to produce a fit to the data using the VDB isochrones when we calculated the reddening zero point using either the SFD maps or the Cacciari (1984) RR Lyrae stars, we conclude that our best estimate for the E_{V-I} zero point is 0.15 mag, giving an average $E_{V-I} \sim 0.24$ for the cluster as a whole. This value falls approximately 1.5 σ below the estimate by Cacciari (1984) and the value tabulated by Harris (1996).

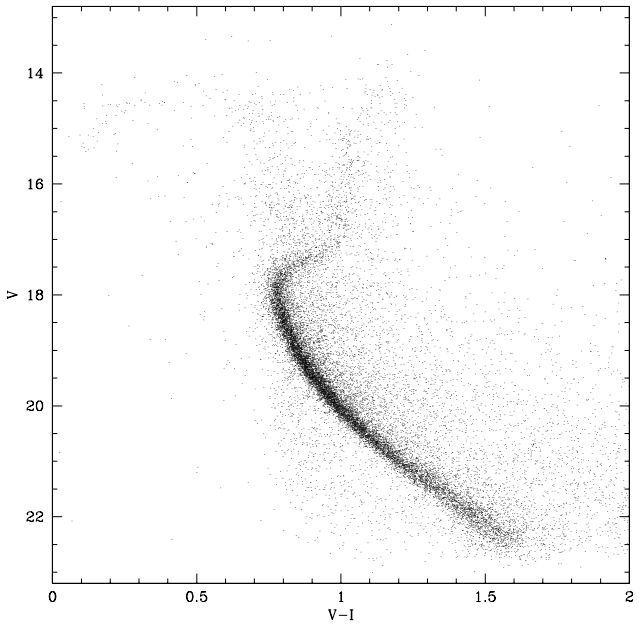

FIG. 9.—Internally dereddened CMD of NGC 3201. V and $V-I$ indicate the location of the data points after the differential reddening, with respect to the fiducial region, was corrected for, i.e., after the inverse values of Fig. 4 were applied to the data. No reddening zero point is applied to the data in this plot.

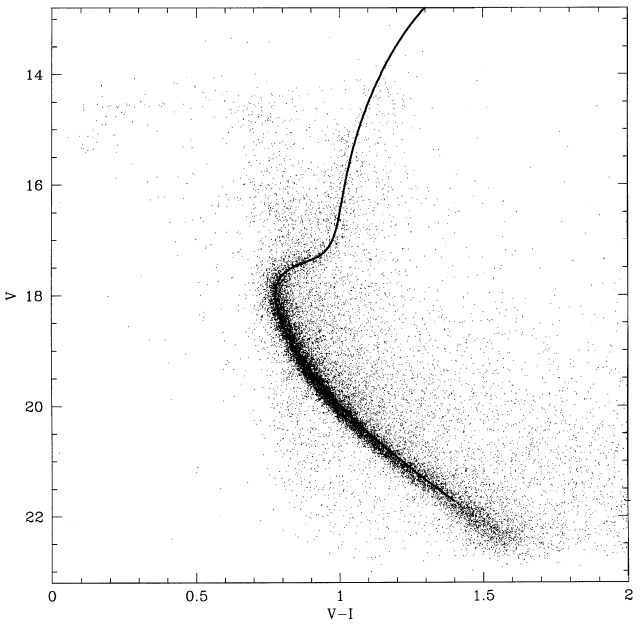

FIG. 10.—Best fit to our data produced by the VDB isochrones. For this fit, [Fe/H] = −1.41, $d \sim 4.5$ kpc, the age is 18 Gyr, and the reddening zero point E_{V-I}, to be added to the values in Fig. 4, is ∼0.15. The average E_{V-I} for the cluster is approximately 0.24 in this plot.

We could force our reddening zero point to agree with these past results by applying a systematic shift of our I magnitudes of 0.08 to brighter values, which would give a distance to NGC 3201 of 4.8 kpc. We have, however, no reason to adopt such a shift. The transformations to standard magnitudes, as well as the application of the aperture corrections (see § 2.1), underwent repeated thorough examinations and appear to be correct. Since no other indication throughout our data reduction and analysis suggests a systematic error in the I-band magnitudes either, we simply

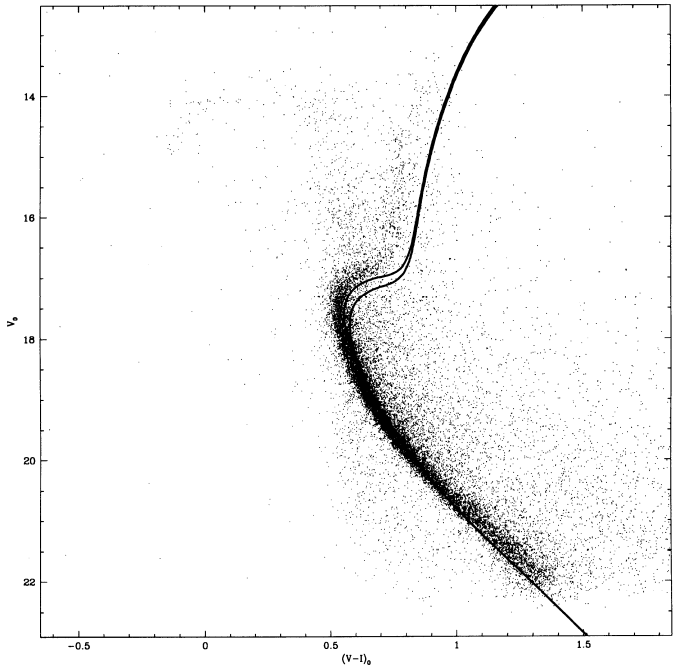

FIG. 11.—CMD of NGC 3201, dereddened to the value of $E_{V-I} = 0.325$ (Harris 1996), plus the isochrones for ages 12 (*top*) and 14 (*bottom*) Gyr with values of [Fe/H] = −1.54 (closest value to Harris' −1.58) and $d = 5.2$ kpc. The agreement between data and fit is better in Fig. 10.

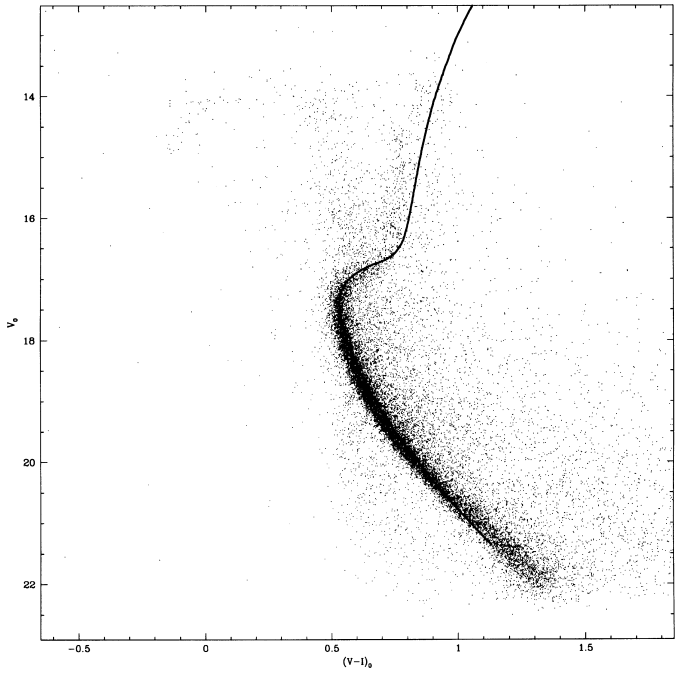

FIG. 12.—Ft to the data dereddened by adopting the E_{V-I} zero point of 0.24, using Cacciari's (1984) RR Lyrae stars, and applying our reddening map. Here [Fe/H] = −2.01 (much lower than literature values), the age is 14 Gyr, and the distance modulus is 13.4. As one can see, the fit fails to reproduce the loci of the data points. We therefore conclude that the reddening zero point of Fig. 10 is correct.

cannot justify adjusting our I magnitudes to compensate for the 1.5 σ effect described above.

5. SUMMARY AND CONCLUDING REMARKS

In the process of finding eclipsing binary stars in NGC 3201, we noticed the existence of variable reddening of up to 0.2 mag in E_{V-I} on a scale of arcminutes. Using our internal dereddening method outlined in § 2.2, we created an extinction map, which is shown in Figures 3 and 4. Applying the map to our raw data (Fig. 8) significantly improved the appearance of the CMD (Fig. 9).

Comparison between our extinction map and the SFD map of the same region (Fig. 6) showed that the same larger scale features exist in both maps. Our map displays some additional, smaller scale features that are absent in the SFD maps (see Fig. 7).

The E_{V-I} zero point, which needs to be added to the numbers in Fig. 4 to get absolute E_{V-I} values, is 0.15. This value is below literature results (Cacciari 1984; Harris 1996) by approximately 1.5 σ but produced by far the best VDB isochrone fit to the data. The zero point determined with the help of the SFD map gives $E_{V-I} \sim 0.49$ as the average value across NGC 3201. This is higher than the literature values, which supports the statement by Arce & Goodman (1999) that the SFD maps overestimate the reddening in regions of high extinction.

The results from this work will be essential in our binary star research, in which high-quality photometry of every binary system is necessary for distance determinations. A vital condition to obtaining these measurements is, of course, knowledge of the exact extinction the star under investigation is suffering.

Furthermore, studies like this may be useful in determining properties of the interstellar medium itself, such as examining a possible dependence of R_V on position in the field of view or giving insight into the distribution and properties of the dust along the line of sight.

This research was funded in part by NSF grants AST 96-19632 and 98-20608. We would like to sincerely thank Alex Athey, Kristin Chiboucas, Robbie Dohm-Palmer, Ivan King, and Don VandenBerg, as well as the anonymous referee, for their help and advice and for pointing out errors during the various stages of the creation of this publication.

REFERENCES

Arce, H., & Goodman, A. 1999, ApJ, 512, L135
Beers, T. C., Flynn, K., & Gebhardt, K. 1990, AJ, 100, 32
Brewer, J. P., Fahlman, G. G., Richer, H. B., Searle, L., & Thompson, I. 1993, AJ, 105, 2158
Cacciari, C. 1984, AJ, 89, 231
Cardelli, J. A., Clayton, G. C., & Mathis, J. S. 1989, ApJ, 345, 245
Côté, P., Welch, D. L., Fischer, P., Da Costa, G. S., Tamblyn, P., Seitzer, P., & Irwin, M. J. 1994, ApJS, 90, 83
Covino, S., & Ortolani, S. 1997, A&A, 318, 40 (CO97)
Da Costa, G. S., Frogel, J. A., & Cohen, J. 1981, ApJ, 248, 612
Forte, J. C., Cellone, S. A., Méndez, M., & Vega, E. I. 1992, ApJ, 388, 383
Gonzalez, G., & Wallerstein, G. 1998, AJ, 116, 765 (GW98)
Harris, W. E. 1996, AJ, 112, 1487
Houdashelt, M. L., Bell, R. A., & Sweigart, A. V. 2000, AJ, 119, 1448
Kaluzny, J., & Krzeminski, W. 1993, MNRAS, 264, 785
Landolt, A. 1992, AJ, 104, 340
Monet, D., et al. 1998, USNO-SA2.0, (Washington: US Naval Obs.)
Piotto, G., Zoccali, M., King, I. R., Djorgosvki, S. G., Sosin, C., Rich, R. M., & Meylan, G. 1999, AJ, 118, 1727
Press, W., Teukolsky, S., Vetterling, W., & Flannery, B. 1992, Numerical Recipes in FORTRAN: The Art of Scientific Computing (2d ed.; Cambridge: Cambridge Univ. Press)
Rosenberg, A., Piotto, G., Saviane, I., & Aparicio, A. 2000, A&AS, 144, 5 (RB00)
Schechter, P. L., Mateo, M., & Saha, A. 1993, PASP, 105, 1342
Schlegel, D. J., Finkbeiner, D. P., & Davis, M. 1998, ApJ, 500, 525 (SFD)
VandenBerg, D., Swenson, F., Rogers, F. J., Iglesias, C. A., & Alexander, D. R. 2000, ApJ, 532, 430 (VDB)

Note added in proof.—The average E_{V-I} value calculated for the SFD map quoted in §§ 3.1, 4.2.2, and 5, as well as in the legend to Figure 6, is wrong. Instead of 487 mmag, the correct value should be 378 mmag. As result of this error, the average E_{V-I} of the difference map (Fig. 7) should read 292 mmag instead of 401 mmag, as quoted in §§ 3.1 and 4.2.2, and in the legend to Figure 7. Our most sincere thanks go out to Douglas Finkbeiner, who pointed out our mistake. The conclusions we reach remain the same, apart from the aforementioned numerical error.